International Journal of Electrical Components and Energy Conversion
2022; 8(1): 1-8
http://www.sciencepublishinggroup.com/j/ijecec
doi: 10.11648/j.ijecec.20220801.11
ISSN: 2469-8040 (Print); ISSN: 2469-8059 (Online)

Analysis on Stator Current Characteristics in Synchronous Generators Under Dynamic Rotor Interturn Short Circuit Fault

Yuan Xing-hua[1, 2], Qiu Ming-hao[1], Jiang Meng-ya[1], He Yu-ling[1, 3, *], Wan Shu-ting[1], Tang Gui-Ji[1]

[1]Department of Mechanical Engineering, North China Electric Power University and Hebei Key Laboratory of Electric Machinery Health Maintenance & Failure Prevention, Baoding, China
[2]Baoding Yunhui Electric Power Equipment Technology Co., LTD, Baoding, China
[3]Suzhou Research Institute, North China Electric Power University, Suzhou, China

Email address:
heyuling1@163.com (He Yu-ling)
[*]Corresponding author

To cite this article:
Yuan Xing-hua, Qiu Ming-hao, Jiang Meng-ya, He Yu-ling, Wan Shu-ting, Tang Gui-Ji. Analysis on Stator Current Characteristics in Synchronous Generators Under Dynamic Rotor Interturn Short Circuit Fault. *International Journal of Electrical Components and Energy Conversion*. Special Issue: *Electro-Mechanical Coupling Problems in Electric Machines*. Vol. 8, No. 1, 2022, pp. 1-8.
doi: 10.11648/j.ijecec.20220801.11

Received: June 4, 2022; **Accepted**: June 24, 2022; **Published**: July 5, 2022

Abstract: Rotor interturn short circuit (RISC) is a common electrical fault in synchronous generators. By far, scholars have carried out a lot of researches on static rotor interturn short circuit (SRISC), while dynamic rotor interturn short circuit (DRISC) is rarely taken into account. This paper analyzes the stator current characteristics before and after DRISC fault in synchronous generators. First, the expressions of the air-gap flux density respectively in normal, SRISC, and DRISC cases, are derived. Then the two-dimensional finite element model is established to analyze the stator current under the aforementioned three conditions. Finally, experiments are carried out on the CS-5 prototype generator to test the stator currents. The experimental results are consistent with the theoretical analysis and the finite element calculation data. It is shown that the occurrence of the dynamic rotor interturn short circuit will reduce the root mean square value as well as the odd harmonics of the magnetic flux density and the stator current, while at the meantime it will increase the new generated even harmonics. Compared with the static short circuit, the current curve of the stator phase shows an obvious "peak". With the aggravation of the short circuit degree between dynamic turns, the effective value of current and the odd harmonics will be decreased. The stator current in the dynamic rotor interturn short circuit cases is generally between those of normal condition and static rotor interturn short circuit case.

Keywords: Synchronous Generator, Dynamic Rotor Interturn Short Circuit, Stator Current, Air-Gap Flux Density

1. Introduction

Rotor interturn short circuit (RISC) is a common fault in generators, which can be divided into static rotor interturn short circuit and dynamic rotor interturn short circuit [1]. Studies have shown that when RISC develops to a certain extent, the drop of the terminal voltage will lead to a strong excitation, causing a significant increase in the exciting current. In addition, there will be unbalanced magnetic pulls on the rotor and uneven heat on the two sides, resulting in the thermal bending and the rotor vibration, due to the asymmetry of the N and S pole windings after short circuit. In severe cases, it may burn the bearing bushes, cause the magnetization of main shaft, and lead to a grounding fault [2-5].

In actual operations, the dynamic interturn short circuit of the exciting windings is in relation to the rotor's frequency and vibration, and may occur due to centrifugal force of winding and the variation of generator vibration intensity [6]. DRISC can be divided into two types. The first refers to the fact that during the rotation of the rotor, the windings come into close contact with high pressure under the centrifugal force, resulting in an interturn short circuit at the worn insulation of the line turns [7]. As the rotor speed decreases, this close contact pressure will decrease and the short circuit condition will disappear, i.e., the transient

interturn short circuit phenomenon occurs only when the rotor speed falls within a certain range. The other refers to a single or periodic interturn short circuit at a specific rotation frequency when the rotation frequency and vibration characteristics of the rotor change. As can be seen, DRISC only exists in a certain phase of rotor rotation, belonging to the period of failure development, but may develop into a stable RISC fault after long time running [8-10].

At present, many scholars at home and abroad have carried out a lot of mechanical and electrical characteristics analysis of the RISC fault. Q. Bin et al. found that the RISC fault of synchronous generator causes an increased excitation current [11]. He Yuling et al. obtained the effect of fault parameter development on the circulating current characteristics by analyzing the air-gap magnetic flux density under RISC [12]. Wan Shuting et al. established the differential equation by modeling the magnetoresistive network of the generator, finding that the even harmonic currents would appear in the stator winding when RISC occurs [13]. Chen Weiliang et al. proposed a modal analysis identification method for end windings based on the perturbation method for multi-cyclic symmetric structure to better avoid the natural frequency around 100 Hz [14]. Wu Yucai et al. established the air-gap magnetic flux density model for the cross influence of mechanical-electrical faults on generators and found that there is no single correspondence between RISC fault and the rotor fundamental frequency vibration amplitude [15]. Cameron A. W. W. et al. performed insulation resistance tests at elevated voltage in order to achieve a non-destructive prediction of breakdown voltage at the weakest point in the winding [4]. Li Junqing et al. analyzed the harmonic variation characteristics of the electromagnetic quantities and the pulsation characteristics of torque of a double fed induction generator under RISC [16]. D. R. Albright et al. used the method of measuring the air-gap magnetic flux density change rate while the rotor was at operating speed to achieve the detection of RISC [17]. G. J. Li et al proposed a fault model for RISC and analyzed the variation trends of the stator winding current and the exciting current [18].

The above literature provides a good basis for the detection and diagnosis of RISC fault. However, most of literature is devoted to the analysis of the fault characteristics after the development of a certain level of interturn short circuit (i.e. static interturn short circuit). There is still room for further development in the area of fault tracing and the differentiation of signature fault characteristics of DRISC. In fact, DRISC do occur from time to time due to a combination of changing operating conditions and centrifugal force. Therefore, it is not complete for the actual operation of the generator that considering only the static interturn short circuit of the excitation winding. The analysis of key fault characteristic parameters such as stator current characteristics under DRISC is important to complement the fault diagnosis criteria for online monitoring of rotor windings, identify faults more quickly and improve diagnostic accuracy.

This paper studies the stator current characteristics of generator under DRISC, and find out the differences from the normal condition and the static interturn short circuit cases, to improve the RISC criterion system on the existing basis.

2. Theoretical Analysis

Although DRISC is a transient process, the electromagnetic parameters change in a similar way to the static interturn short circuit at the moment that the short circuit actually occurs. For the ease of explanation and understanding, this paper starts with the electromagnetic variation law of static interturn short circuit, then on this basis the difference between dynamic and static interturn short circuit will be analyzed, exploring the effect of this difference on the variation law of electromagnetic parameters.

2.1. Impact of DRISC on MFD

MFD can be obtained by multiplying the magnetomotive force (MMF) by the permeance per unit area (PPUA). As shown in Figure 2(a), the air-gap MFD at any circumferential mechanical angle α in stator coordinates can be written as:

$$B(\alpha,t) = f(\alpha,t)\Lambda_0 \tag{1}$$

where f is the air-gap synthetic MMF, obtained by vector synthesis of the main MMF (rotor MMF) and the armature reaction MMF (stator MMF), Λ_0 is PPUA, numerically equal to μ_0/g_0, g_0 is the radial air-gap length.

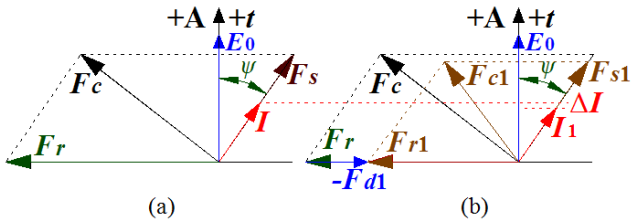

Figure 1. *MMF vectors before and after short circuit: (a) normal condition, (b) short circuit case.*

RISC affects the MFD by influencing air-gap MMF. When RISC occurs, the number of ampere-turns at the pole where the short circuit is located decreases, resulting in an asymmetric MFD at both ends. The change in the main MMF before and after the short circuit is shown in Figure 2(b) and (c), where T is dynamic interturn short circuit period, k is the normal part duty cycle, $\triangle h_1$ and $\triangle h_2$ are the instantaneous pulsed MMF generated when the normal and short circuit states are transformed into each other, and the value of the pulse is theoretically infinite. The corresponding stator and rotor MMF vectors variations are shown in Figure 1(a) and (b), where F_r, F_s and F_c are respectively the 1st harmonic of main MMF, armature reaction MMF and 1st harmonic of air-gap synthetic MMF, E_0 is the no-load potential, I is the phase current under normal condition, ψ is the internal work angle of the generator. Parameters with the number 1 in the lower corner of Figure 1(b) are used to represent the parameters after RISC.

For ease of analysis, the occurrence of RISC can be equated to the addition of a reverse current to the normal excitation current to offset the effect of the short circuit on the original wire turns [14], i.e., an inverse MMF is added to offset the

MMF of normal operating. According to Gauss' flux theorem, the expression for the additional MMF generated by the reverse current can be written as:

$$F_d(\theta_r)=\begin{cases}-\dfrac{I_f n_m(2\pi-\alpha_r)}{2\pi} & \beta' \le \theta_r \le \beta'+\alpha_r \\ \dfrac{I_f n_m \alpha_r}{2\pi} & \theta_r < \beta', \theta_r > \beta'+\alpha_r\end{cases} \tag{2}$$

where I_f is exciting current, n_m is the number of the short circuit turns, θ_r is the circumferential angle of the rotor surface, β' is the beginning angle of the slot where the interturn short circuit takes place, α_r is the angle between the two slots where the short circuit turns are in, which are shown in Figure 1(a).

The Fourier series expansion of the additional MMF $F_d(\theta_r)$ is:

$$\begin{cases}F_d(\theta_r)=A_0+\sum_{n=1}^{\infty}\left[A_n\cos(n\theta_r)+B_n\sin(n\theta_r)\right] \\ A_0=\dfrac{1}{2\pi}\int_0^{2\pi}F_d(\theta_r)d\theta_r=0 \\ A_n=\dfrac{1}{\pi}\int_0^{2\pi}F_d(\theta_r)\cos(n\theta_r)d\theta_r=-\dfrac{I_f n_m\left[\sin\left(n(\alpha_r+\beta')\right)-\sin(n\beta')\right]}{n\pi} \\ B_n=\dfrac{1}{\pi}\int_0^{2\pi}F_d(\theta_r)\sin(n\theta_r)d\theta_r=\dfrac{I_f n_m\left[\cos\left(n(\alpha_r+\beta')\right)+\cos(n\beta')\right]}{n\pi}\end{cases} \tag{3}$$

As shown in the figure, static short circuit can be equated to the addition of a reverse step MMF to the normal MMF, and its superimposed MMF can be expressed as:

$$f(\alpha,t)=\begin{cases}\sum_{n=1}^{\infty}F_n\cos(n\omega t-p\alpha) & \cdots\cdots\text{Normal} \\ \sum_{n=1}^{\infty}F_n\cos(n\omega t-p\alpha)-\sum_{m=1}^{\infty}F_{dm}\cos(m\omega t-p\alpha) & \cdots\text{RISC}\end{cases} \tag{4}$$

where F_n is the nth harmonic amplitude of MMF, F_{dm} is the mth harmonic amplitude generated by the short circuit turns, and n represents odd numbers, m represents all natural numbers.

According to Eq. (4), air-gap MMF of generator only has odd harmonics under normal working condition. Even harmonics will appear on the basis of normal odd harmonics after static RISC. Overall, the reduction in the number of effective ampere turns after RISC results in the decrease of the overall amplitude of MMF.

The reverse MMF signal generated by DRISC is a transient signal, which can be seen as a pulse signal. On the whole, it can be regarded as adding a reverse square wave pulsed MMF on the basis of normal MMF, which is expressed as follows:

$$f(\alpha,t)=\begin{cases}\sum_{n=1}^{\infty}F_n\cos(n\omega t-p\alpha) & \cdots\cdots(i-1)T<t<(i-1+k)T \\ \Delta h_1 & \cdots\cdots t=(i-1+k)T \\ \sum_{n=1}^{\infty}F_n\cos(n\omega t-p\alpha)-\sum_{m=1}^{\infty}F_{dm}\cos(m\omega t-p\alpha) & \\ \cdots\cdots & (i-1+k)T<t<iT \\ \Delta h_2 & \cdots\cdots t=iT\end{cases} \tag{5}$$

where I represents all natural numbers, T is the DRISC cycle, k is the duty cycle of the normal part.

As can be seen from Eq. (5), MMF should also have even harmonics in addition to the original odd harmonics after DRISC. An infinite MMF pulse signal will appear at the moment when the short circuit state and the normal state are transformed into each other in dynamic short-circuit cycle. However, the amplitude of MMF under DRISC condition should be between MMF amplitude under normal condition and RISC condition (static RISC can be considered as a special case of DRISC with a duty cycle of 1). With the variation of normal condition duty cycle in DRISC cycle, the fluctuation in amplitude of MMF changes accordingly.

For the convenience of analysis, static air-gap eccentricity is not considered in this paper, so the PPUA Λ_0 in Eq. (1) is kept constant. Correspondingly, the air-gap MFD expression can be written as Eq. (6).

$$B(\alpha,t)=\begin{cases}\sum_{n=1,3,5\cdots}^{\infty}F_n\cos(n\omega t-p\alpha)\Lambda_0 & \cdots\cdots\text{Normal} \\ \left[\sum_{n=1,3,5\cdots}^{\infty}F_n\cos(n\omega t-p\alpha)-\sum_{m=1,2,3\cdots}^{\infty}F_{dm}\cos(m\omega t-p\alpha)\right]\Lambda_0 & \\ \cdots\cdots & \cdots\cdots\text{SRISC} \\ \begin{cases}\sum_{n=1,3,5\cdots}^{\infty}F_n\cos(n\omega t-p\alpha)\Lambda_0 & \cdots(i-1)T<t<(i-1+k)T \\ \Delta h_1\Lambda_0 & \cdots\cdots t=(i-1+k)T \\ \left[\sum_{n=1,3,5\cdots}^{\infty}F_n\cos(n\omega t-p\alpha)-\sum_{m=1,2,3\cdots}^{\infty}F_{dm}\cos(m\omega t-p\alpha)\right]\Lambda_0 & \\ \cdots\cdots & (i-1+k)T<t<iT \\ \Delta h_2\Lambda_0 & \cdots\cdots t=iT\end{cases} & \\ \cdots\cdots & \cdots\cdots\text{DRISC}\end{cases} \tag{6}$$

Combining Eq. (6) with the previous analysis, it shows that: the amplitude of the air-gap MFD will be decreased under DRISC, and new even harmonics will appear on the basis of the original odd harmonics. The amplitude of the odd harmonics will be decreased, while the even harmonics will be increased with the aggravation of the short circuit. There is a pulse at the moment of transition between short circuit and normal condition. The overall amplitude of MFD under DRISC is between those of normal condition and SRISC case.

2.2. Analysis of Stator Current Characteristics

According to Faraday's law of electromagnetic induction and Ohm's law, the expression of the phase current can be written as:

$$I(\alpha_m,t)=\frac{B(\alpha_m,t)\ lv}{Z} \tag{7}$$

where l is the effective length of the stator winding which cuts the magnetic flux lines and is approximately equal to the axial length of the stator core; Z is the reactance of the single-phase winding, v is the linear velocity of the magnetic field rotation [19].

Substituting Eq. (6) into Eq. (7), the expressions for the

stator current under normal, SRISC and DRISC can be further written as Eq. (8).

$$I(\alpha,t)=\begin{cases}\left[\sum_{n=1,3,5\cdots}^{\infty}F_n\cos(n\omega t-p\alpha)\right]lv\Lambda_0/Z\cdots\cdots\text{Normal}\\ \left[\sum_{n=1,3,5\cdots}^{\infty}F_n\cos(n\omega t-p\alpha)-\sum_{m=1,2,3\cdots}^{\infty}F_{dm}\cos(m\omega t-p\alpha)\right]lv\Lambda_0/Z\cdots\cdots\text{SRISC}\\ \begin{cases}\left[\sum_{n=1,3,5\cdots}^{\infty}F_n\cos(n\omega t-p\alpha)\right]lv\Lambda_0/Z\cdots\cdots(i-1)T<t<(i-1+k)T\\ \Delta h_1 lv\Lambda_0/Z\cdots\cdots t=(i-1+k)T\end{cases}\\ \begin{cases}\left[\sum_{n=1,3,5\cdots}^{\infty}F_n\cos(n\omega t-p\alpha)-\sum_{m=1,2,3\cdots}^{\infty}F_{dm}\cos(m\omega t-p\alpha)\right]lv\Lambda_0/Z\cdots\cdots(i-1+k)T<t<iT\\ \Delta h_2 lv\Lambda_0/Z\cdots\cdots t=(i-1+k)T\end{cases}\\ \cdots\cdots\text{DRISC}\end{cases}\tag{8}$$

As can be seen from Eq. (8), the current of stator under DRISC fault depends mainly on the air-gap MFD and the rotor speed. Since the degree of DRISC is generally small, it will result in very little change in the rotor speed. Therefore, to ease the analysis, the rotor speed is considered to be constant in this paper. Thus, the change in MFD becomes a primary factor in determining the magnitude of the stator current, and its variation trend should be consistent with the current change tendency.

Correspondingly, compared with normal condition, the even harmonics of the stator current will appear on the basis of the original odd harmonics under DRISC condition. The effective value of the stator current will be decreased with the aggravation of the DRISC degree. In a DRISC cycle, the infinite pulse of current occurs at the moment transition between the short circuit and normal states. However, the infinite pulse signal appears as a "spike" in the simulation and the experiment due to the discrepancy between the theoretical analysis and the simulation and experiment. And according to the above analysis, there will be a "spike" that reduces the current amplitude in the moment of transformation from normal to short circuit condition, and a "spike" that increases the current amplitude in the moment of transformation from short circuit to normal condition. The absolute value of this "spike" will be increased as the dynamic short circuit increases. In terms of the overall amplitude of the current, the effective value under DRISC is between those of normal condition and SRISC case.

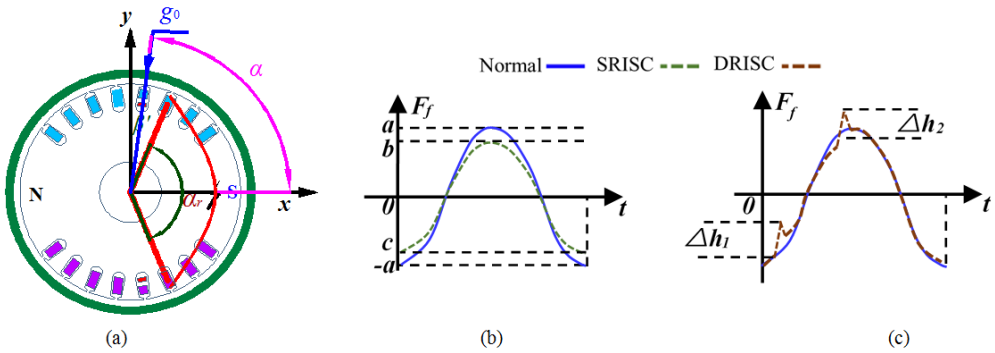

Figure 2. *Rotor interturn short circuit and magnetic potential diagram: (a) rotor interturn short circuit, (b) air-gap MMF in SRISC case, (c) air-gap MMF in DRISC case.*

3. FEA and Experimental Validation

3.1. Object and Method

FEA and experimental verifications of DRISC and SRISC are taken on a CS-5 non-salient prototype generator. The experimental rig is shown in Figure 3(a) and the FEA model is shown in Figure 3(b), where L_1-L_5 are the interturn short circuit taps of the exciting winding: 0% (L_1), 5% (L_2), 10% (L_3), 15% (L_4), 100% (L_5).

SRISC experiment is realized by directly connecting the taps. The DRISC switch is controlled by a DC solid state relay in conjunction with an adjustable duty cycle PWM square wave generator, the corresponding trigger circuit is shown in Figure 3(d). The output voltage of the DC power supply is truncated and commutated by PWM to output a square wave voltage signal with a period of 20ms and a 15% duty cycle for the short circuit section. The signal triggers the opto-coupler within the DC solid state relay to realize the periodical opening and closing of short circuit without contact, so that DRISC can be accurately simulated.

In order to make the setup of the DRISC in FEA identical to that in the experiment, the physical model coupled to the external circuit is used to simulate the fault. The external coupling circuit of the exciting winding and the armature

winding are shown in Figure 3(e) and (f), where S-A1 is a short circuit trigger switch, which sets the trigger voltage interval [Von, Voff] and cooperates with the pulse voltage source to control the short circuit, realizing the simulation of DRISC. The pulse time setting for a DRISC period is shown in Figure 3(c).

Table 1. *CS-5 fault analog generator parameters.*

Parameters	Values	Parameters	Values
Rated power	5KW	radial air-gap length	1.2mm
Rated exciting current	5A	Stator slots	36
Rated rotating speed	3000r/min	Rotor slots	16
Pole-pairs	1	Exciting turns	480
Parallel branches	2	Synchronous reactance	2.03Ω
Power factor	cosφ=0.8	Stator core length	130mm
Stator core outer diameter	250.5mm	Stator core inner diameter	145mm

In FEA, the simulation of different short circuit degrees is achieved by varying the number of turns of the winding LF and the short circuit winding LF short as well as the resistance values of the corresponding resistors R_w and R_f. In Figure 3(c), T_d is the delay time, T_r is the rise time, T_f is the fall time, P_w is the pulse width, V_{on} is the trigger voltage of the voltage-controlled switch. When the voltage value of the pulse voltage source is greater than V_{on}, switch S_A1 operates, i.e., the RISC occurs. V_{off} is the cut-off voltage of the voltage-controlled switch. When the voltage value of the pulse voltage source is less than V_{off}, switch S_A1 breaks, i.e., the exciting circuit returns to normal. The duty cycle of the short circuit and the frequency of DRISC are changed by adjusting the values of P_w and Period. By setting the above parameters, an external circuit of DRISC with a period of 20ms and a duty cycle of 15% for the short circuit section is generated, which is the same as the settings in the experiment.

Four groups of normal, SRISC-5% (L_1-L_2), DRISC-5% (L_1-L_2) and DRISC-10% (L_1-L_3) were measured and calculated in experiments and FEA.

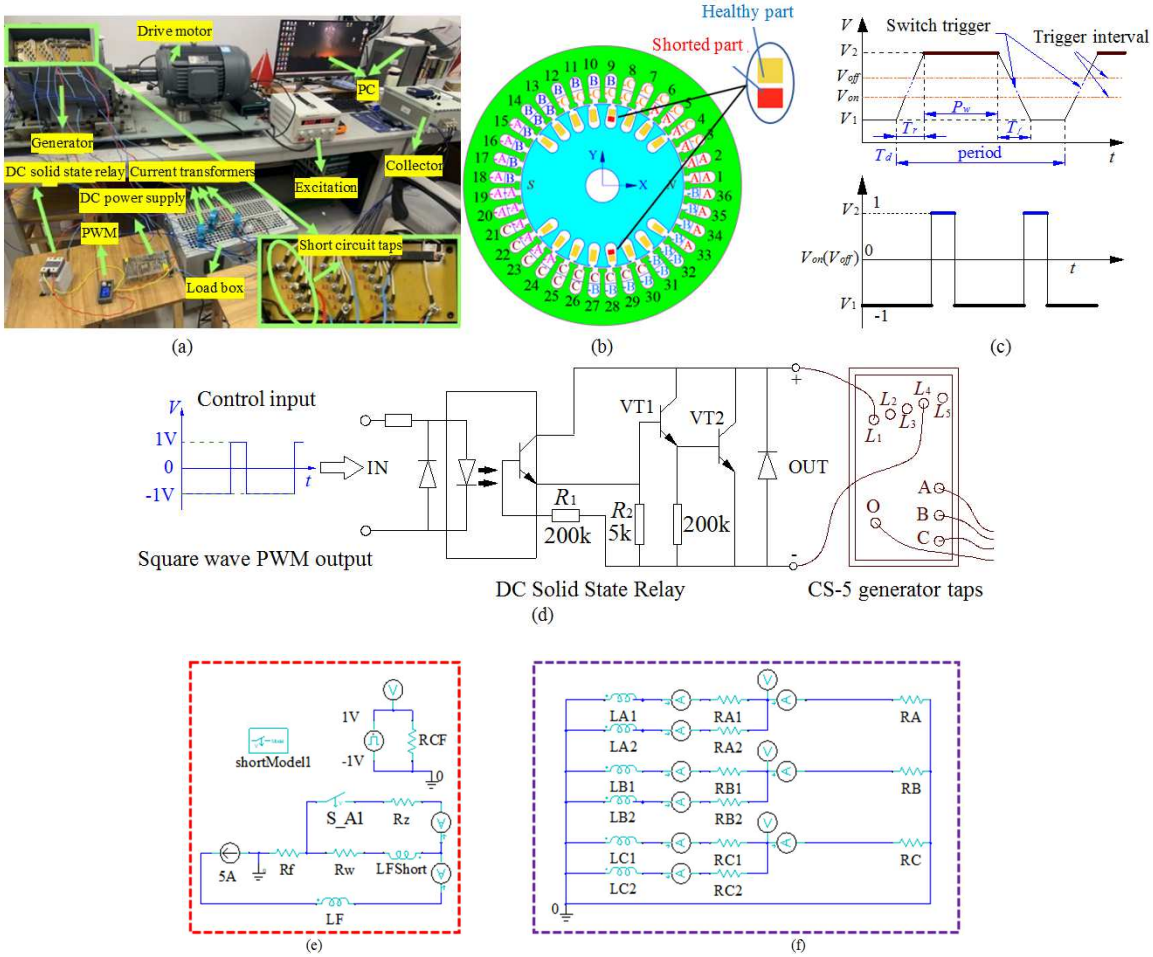

Figure 3. *Simulation and experiment set up: (a) experimental table, (b) FEA model, (c) sequence diagram of short-circuit switch triggering voltage, (d) DRISC trigger circuit, (e) exciting winding coupling circuit model, (f) stator winding coupling circuit model.*

3.2. Results and Discussion

The finite element calculation results of the air-gap MFD before and after the short circuit are shown in Figure 3, where "Normal", "S-5", "D-5", "D-10" represent normal, SRISC-5%, DRISC-5% and DRISC-10%, respectively. As can be seen in Figure 4, RISC will lead to a reduction of the air-gap MFD, and the overall air-gap MFD curve will be "compressed". The MFD amplitude under DRISC is between those of normal and SRISC

conditions, and is close to the amplitude under normal conditions. Comparing the curve D-5 with D-10 in Figure 4(a), it can be seen that the amplitude of MFD will be decreased as DRISC increases. A transient pulse signal appears at the moment when normal and short circuit are transformed into each other, and such pulse will be increased as DRISC goes severer.

Fast Fourier Transform is performed on MFD in the DRISC-5% case, and the spectrum histogram is shown in Figure 4(b). It can be seen that the second and the fourth harmonics will be increased after the short circuit, but the first and the third harmonics will be decreased. Such developing trend is the same as SRISC, with only the variation magnitude different. Due to space limit, the harmonic changes after SRISC are not repeated in this paper.

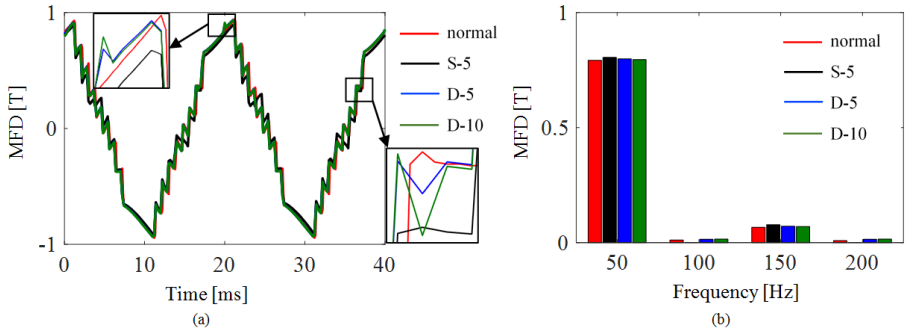

Figure 4. *Simulation results of magnetic flux density: (a) MFD at different operating conditions, (b) MFD spectrogram.*

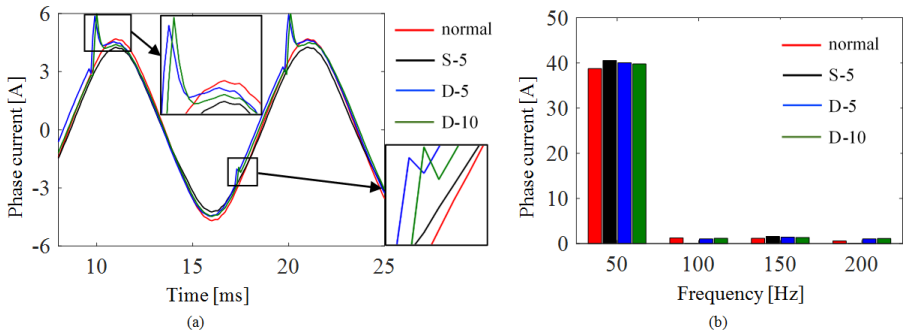

Figure 5. *Simulation analysis results of stator winding current: (a) phase current at different operating conditions, (b) Phase current spectrogram.*

Table 2. *Spectrum analysis of flux density and stator current.*

Conditions	1st 50HZ		2nd 100HZ		3rd 150HZ		4th 200HZ		RMS	
	MFD (T)	Current (A)	MFD (T)	Current (A)	MFD (T)	Current (A)	MFD (T)	Current (A)	MFD (T)	Current (A)
S-5	0.7918 —	38.7157 —	0.0112 —	1.26326 —	0.0670 —	1.17060 —	0.0062 —	0.59273 —	0.5697 —	26.86138 —
Normal	0.8047	40.5429	0	0	0.0781	1.58032	0	0	0.5837	29.80139
D-5	0.7988 ↓	40.0417 ↓	0.0014 ↑	1.05875 ↑	0.0713 ↓	1.44158 ↓	0.0019 ↑	1.04832 ↑	0.5801 ↓	29.00590 ↓
D-10	0.7952	39.7617	0.0052	1.19154	0.0698	1.36654	0.0026	1.13401	0.5736	28.85344

Finite element calculation results of the stator phase current changes before and after the short circuit are shown in Figure 5. It can be seen that the effective value of the phase current after DRISC decreases and presents a "compression" state. Comparing the three curves as well as their corresponding RMS of Normal, S-5 and D-5 in Figure 5(a) with each other, it is found that the current curve and RMS of DRISC are between those of normal and SRISC cases under the same short circuit degree. At the moment when normal and the dynamic short circuit condition are transformed into each other, a transient pulse of current appears, i.e., a "spike", which will appear, and such “spike” will be increased as the short circuit degree increases. Compared with the case of SRISC in the 9th Figure in Ref. [19], it can be seen that the phase current variation is slip, while the current under DRISC will show the aforementioned “spike”. Consequently, such “spike” can be used as a criterion to identify DRISC from SRISC.

The spectral analysis of the stator current derived from the simulation is shown in Figure 5(b). According to Figure 5(b) and Table 2, the first and the third harmonic amplitudes will be decreased, while the second and the fourth harmonics will newly appear after DRISC. With the intensification of the degree of DRISC, the amplitude of the first and the third harmonics will be decreased, while the second and the fourth harmonics will be increased. Such result is consistent with the theoretical analysis obtained rom Eq. (8).

The time domain waveforms and the spectrum histograms of the stator phase current under four experimental conditions of normal, SRISC-5%, DRISC-5% and DRISC-10% are shown in Figure 6. At the crest of the curve in Figure 6(a), the induced current is "Normal", "D-5", "D-10" and "S-5" in the descending order.

Comparing the three current curves of Normal, S-5 and D-5 in

Figure 6(a) and their corresponding RMS with each other, it is found that the effective value of the stator current after DRISC is between normal and SRISC under the same short circuit degree. The current curve shows a significant "spike", which is pretty different from the normal and SRISC conditions. As DRISC gets worse, the "spike" will become higher. The first and the third harmonics of the phase current will be decreased, while the second and the fourth harmonics will be newly induced after DRISC. As the degree of short circuit intensifies, the first and the third harmonics will be decreased, but the second and the fourth harmonics will be increased. The above conclusions are consistent with the previous theoretical analysis and the finite element analysis data.

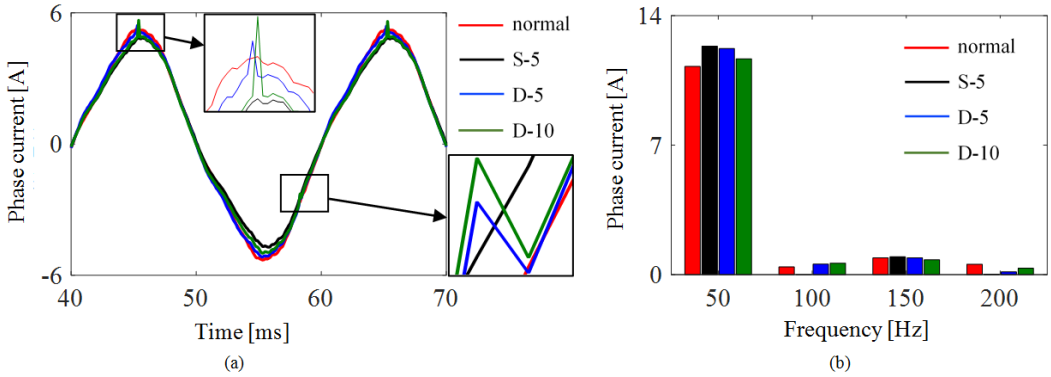

Figure 6. *Experimental results of stator winding current: (a) phase current at different operating conditions, (b) phase current spectrogram.*

Table 3. *Spectrum analysis of measured stator current.*

Conditions	1st 50HZ		2nd 100HZ		3rd 150HZ		4th 200HZ		RMS	
S-5	11.2477	—	0.41107	—	0.90012	—	0.5577	—	31.953	—
Normal	12.3464		0.00107		0.95316		0.0163		35.055	
D-5	12.2180	↓	0.56218	↑	0.90971	↓	0.1412	↑	34.663	↓
D-10	11.6612		0.61497		0.80122		0.3435		33.114	

4. Conclusion

This paper presents the theoretical analysis, the finite element analysis, and the experimental verification on the stator current characteristics before and after DRISC. It is shown that:

(1) After DRISC the air-gap MFD curve shows a "compression" trend and the amplitude will be decreased. The odd harmonics such as the first and the third harmonics will be decreased, while the even harmonics such as the second and the fourth harmonics will be generated. As the DRISC degree increases, the odd harmonics of MFD will be decreased while the even harmonics will be increased.

(2) The overall amplitude of the stator phase current under DRISC is between those of the normal condition and SRISC case. As the DRISC increases, the effective value of the stator current and the odd harmonics will be decreased, while the even harmonics will be increased.

(3) Compared with SRISC, the current curve of DIRSC shows two significant "spikes", which will become higher as the degree of dynamic short circuit increases.

The results of this paper are important supplements to the existing research on RISC and provide a basis for the effective determination between DRISC and SRISC, which is of significance for the detection and the diagnostic refinement of RISC in large generators.

Acknowledgements

This work is supported by the National Natural Science Foundation of China (No. 52177042), the Natural Science Foundation of Hebei Province (E2020502031), the Chinese Research Funds for the Central Universities (2017MS151), Suzhou Social Developing Innovation Project of Science and Technology (SS202134), and the Hebei Provincial Top Youth Talent Support Program ([2018]-27).

References

[1] Li Junqing. Research on Dynamic Interturn Short Circuit Fault Location of Exciting Winding in Turbine Generators [J] Proceedings of the CSEE, 2015, 35 (07): 1775-1781.

[2] BAN Guo-bang, LI Yong-gang, ZHAO Li-jin, LI Xiao-jun. Research on joint diagnostic methods of dynamic rotor winding inter-turn short circuit fault based on the electromagnetic properties [J] Journal of North China Electric Power University, 2014, 41 (03): 32-35.

[3] Gandhi, A., Corrigan, T., Parsa, L. Recent Advances in Modeling and Online Detection of Stator Interturn Faults in Electrical Motors [J]. IEEE Transactions on Industrial Electronics, 2011, 58 (5): 1564-1575.

[4] Cameron A. W. W. Diagnoses of A-C Generator Insulation Condition by Nondestructive Tests includes discussion [J]. Power Apparatus and Systems, Part III: Transactions of the American Institute of Electrical Engineers, 1952, 71 (1): 263-269.

[5] Zhang Chao, Xia Li, Wu Zhenguo, etc. Distinguishing stator winding inter-turn short-circuit from asymmetrical operation of synchronous generator [J]. Electric Power Automation Equipment, 2011, 31 (04): 41-46.

[6] HAO Liangliang, WU Junyong, CHEN Zhanfeng, SONG Honglei. Mechanism of Effects of Inter-turn Short Circuits in Field Windings on large Turbo-generator Viberation. [J]. Automation of Electric Power Systems, 2014, 38 (04): 25-31+50.

[7] ZHANG Zhengping, LIU Shi. Online diagnosis of interturn short circuit for large turbine generator's rotor. [J]. Electric Power Automation Equipment, 2012, 32 (08): 148-152.

[8] ZHANG Chao, XIA Li, WU Zheng-guo, HUANG Hai, WANG Jia-lin. Analysis on Fault Characteristics Law of Interturn Short Circuit in Synchronous Generator Rotor Winding. [J]. High Voltage Engineering, 2010, 36 (06): 1506-1512.

[9] ZHAO Hong-sen, GE Bao-jun, TAO Da-jun, YANG Kun, XING Guang. Investigation on Stator Winding Inter-turns Short Circuit Fault Diagnosis [J]. Journal of Harbin University of Science and Technology, 2018, 23 (01): 99-104.

[10] LI Yong-gang, LI He-ming, ZHAO Hua. The new criterion on inter turn short-circuit fault diagnose of steam turbine generator rotor windings. [J]. Proceedings of the CSEE, 2003 (06): 112-116+169.

[11] Q. Bin, X. Wei, L. Nian, et al. Theoretical research on short circuit fault of rotor inner winding in large turbo generator [C] IECON 2012 - 38th Annual Conference on IEEE Industrial Electronics Society. IEEE, 2012: 6218-6223.

[12] HE Yuling. Analysis on Mechanical and Electrical Characteristics of Generator under Air-Gap Eccentricity and Winding Short Circuit Composite Faults. [D]. North China Electric Power University, 2012.

[13] W. Shuting., W. Aimeng, L. Yonggang, et al. Reluctance network model of turbo-generator and its application in rotor winding inter-turn short circuit fault [C] IEEE International Conference on Electric Machines and Drives. IEEE, 2005: 386-390.

[14] CHENG Wei-liang, XU Bo-hou, HUANG Lei. Vibration analysis of stator winding end baskets of large turbo- generator [J]. Journal of Zhejiang University (Engineering Science), 2010, 44 (08): 1558-1561.

[15] WU Yu-cai, LI Yong-gang, LI He-ming, etc. Analysis of Turbine Generator Rotor Vibration Characterisitc Under Electromechanical Compound Faults. [J]. High Voltage Engineering, 2010, 36 (11): 2687-2692.

[16] J. Li, L. Zhang and W. Shi, Fault characteristics of the DFIG rotor inter-turn short circuit considering inherent imbalance and static eccentricity, 2015 IEEE Energy Conversion Congress and Exposition (ECCE), 2015: 971-975.

[17] D. R. Albright. Interturn Short-Circuit Detector for Turbine-Generator Rotor Windings [J]. IEEE Transactions on Power Apparatus and Systems, 1971, PAS-90 (2): 478-483.

[18] G. J. Li et al. Excitation Winding Short-Circuits in Hybrid Excitation Permanent Magnet Motor [J]. IEEE Transactions on Energy Conversion, 2014, 2014, 29 (3): 567-575.

[19] Yu-Ling He, etc. Analysis and simulation on the effect of rotor interturn short circuit on magnetic flux density of turbo–generator. [J]. Journal of Electrical Engineering-Elektrotechnicky Casopis, 2016, 67 (5): 323-333.